

FDR-HS: An Empirical Bayesian Identification of Heterogenous Features in Neuroimage Analysis

Xinwei Sun^{1,6}, Lingjing Hu²(✉), Fandong Zhang^{3,6}, Yuan Yao⁴(✉), and Yizhou Wang^{5,6}

¹ School of Mathematical Science, Peking University, Beijing, 100871, China

² Yanjing Medical College, Capital Medical University, Beijing, 101300, China

³ Key Laboratory of Machine Perception (Ministry of Education), Department of Machine Intelligence, School of Electronics Engineering and Computer Science, Peking University, Beijing 100871, China

⁴ Hong Kong University of Science and Technology and Peking University, China

⁵ National Engineering Laboratory for Video Technology, Key Laboratory of Machine Perception, School of EECS, Peking University, Beijing, 100871, China

⁶ Deepwise Inc., Beijing, 100085, China

Abstract. Recent studies found that in voxel-based neuroimage analysis, detecting and differentiating “procedural bias” that are introduced during the preprocessing steps from lesion features, not only can help boost accuracy but also can improve interpretability. To the best of our knowledge, GSplit LBI is the first model proposed in the literature to simultaneously capture both procedural bias and lesion features. Despite the fact that it can improve prediction power by leveraging the procedural bias, it may select spurious features due to the multicollinearity in high dimensional space. Moreover, it does not take into account the heterogeneity of these two types of features. In fact, the procedural bias and lesion features differ in terms of volumetric change and spatial correlation pattern. To address these issues, we propose a “two-groups” Empirical-Bayes method called “FDR-HS” (False-Discovery-Rate Heterogenous Smoothing). Such method is able to not only avoid multicollinearity, but also exploit the heterogenous spatial patterns of features. In addition, it enjoys the simplicity in implementation by introducing hidden variables, which turns the problem into a convex optimization scheme and can be solved efficiently by the expectation-maximum (EM) algorithm. Empirical experiments have been evaluated on the Alzheimer’s Disease Neuroimage Initiative (ADNI) database. The advantage of the proposed model is verified by improved interpretability and prediction power using selected features by FDR-HS.

Keywords: · Voxel-based Structural Magnetic Resonance Imaging · False Discovery Rate Heterogenous Smoothing · Procedural Bias · Lesion Voxel

Dedicated to Professor Bradley Efron on the occasion of his 80th birthday.

1 Introduction

In recent years, the issue of model interpretability attracts an increasing attention in voxel-based neuroimage analysis of disease prediction, e.g. [9,5]. Examples include, but not limited to, the preprocessed features on structural Magnetic Resonance Imaging (sMRI) images that usually contain the following voxel-wise features: (1) lesion features that are contributed to the disease (2) procedural bias introduced during the preprocessing steps and shown to be helpful in classification [12,3] (3) irrelevant or null features which are uncorrelated with disease label. Our goal is to stably select non-null features, i.e. lesion features and procedural bias with high power/recall and low false discovery rate (FDR).

The lesion features have been the main focus in disease prediction. In dementia disease such as Alzheimer’s Disease (AD), such features are thought to be geometrically clustered in atrophied regions (hippocampus and medial temporal lobe etc.), as shown by the red voxels in Fig. 1 (A). To explore such spatial patterns, multivariate models with Total Variation [10] regularization can be applied by enforcing smoothness on the voxels in neighbor, e.g. the n^2 GFL [16] can stably identify the early damaged regions in AD by harnessing the lesions.

Recently, another type of features called procedural bias, which are introduced during the preprocessing steps, are found to be helpful for disease prediction [12]. Again, taking AD as an example, the procedural bias refer to the mistakenly enlarged Gray Matter (GM) voxels surrounding locations with cerebral spinal fluid (CSF) spaces enlarged, e.g. lateral ventricle, as shown in Fig. 1 (A). This type of features has been ignored in the literature until recently, when the GSplit LBI [12] was targeted on capturing both types of features via a split of tasks of TV regularization (for lesions) and disease prediction with general linear model (with procedural bias). By leveraging such bias, it can outperform models which only focus on lesions in terms of prediction power and interpretability.

However, GSplit LBI may suffer from inaccurate feature selection due to the following limitations in high dimensional feature space:⁷ (1) multicollinearity: high correlation among features in multivariate models [14]; (2) “heterogenous features”: the procedural bias and lesion features differ in terms of volumetric change (enlarged v.s. atrophied) and particularly spatial pattern (surroundingly distributed v.s. spatially cohesive). Specifically, the multicollinearity could select spurious null features which are inter-correlated with non-nulls. Moreover, GSplit LBI fails to take into account the heterogeneity since it enforces correlation on features without differentiation. Such problems altogether may result in inaccurate selection of non-nulls, especially procedural bias. As shown in Fig. 1 (B) and Table 2, the procedural bias selected by GSplit LBI are unstably scattered on regions that are less informative than ventricle. Moreover, the collinearity among features tends to select a subset of features among correlated ones, as discussed in [17]. Such a limitation leads to the ignorance of many meaningful regions (such as medial temporal lobe, thalamus etc.) of GSplit LBI in selecting lesion features, as identified by the purple frames of FDR-HS in Fig. 1 (B).

⁷ Please refer supplementary material for detailed and theoretical discussion

Moreover, the two problems above may get worse as dimensionality grows. In our experiments with a fine resolution ($4 \times 4 \times 4$ of 20,091 features), the prediction accuracy of GSplit LBI deteriorates to 89.77% (as shown in Table 3), lower than 90.91% reported in [12] with a coarse resolution ($8 \times 8 \times 8$ of 2,527 features).

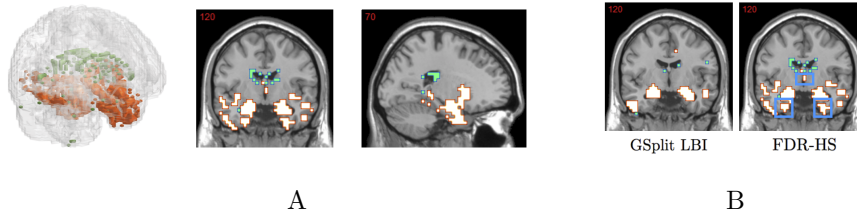


Fig. 1. A: the features selected by FDR-HS (green denotes procedural bias; red denotes lesion features which are geometrically clustered) B: comparison with GSplit LBI

To resolve the problems above, we propose a “two-groups” empirical Bayes method to identify heterogenous features, called FDR-HS standing for “FDR Heterogenous smoothing” in this paper. As a univariate FDR control method, it avoids the collinearity problem by proceeding voxel-by-voxel, as discussed in [7]. Moreover, it can deal with heterogeneity by regularizing on features with different levels of spatial coherence in different feature groups, which remedies the problem of losing spatial patterns that most conventional mass-univariate models suffer from, such as two sample T-test, BH_q [4] and LocalFDR [7]. By introducing a binary latent variable, our problem turns into a convex optimization and can be solved efficiently via EM algorithm like [13]. The method is applied to a voxel-based sMRI analysis for AD with a fine resolution ($4 \times 4 \times 4$ of 20,091 features). As a result, our proposed method exhibits a much stabler feature extraction than GSplit LBI, and achieves much better classification accuracy at 91.48%.

2 Method

Our dataset consists of p voxels and N samples $\{x_i, y_i\}_1^N$ where x_{ij} denotes the intensity value of the j^{th} voxel of the i^{th} sample and $y_i = \{\pm 1\}$ indicates the disease status (-1 denotes AD). The FDR-HS method is proposed to select non-null features. Such method is the combination of “two-groups” model and heterogenous regularization, which is illustrated in Fig. 2 and discussed below. **Model Formulation.** Assuming for each voxel $i \in \{1, \dots, p\}$, the statistic z_i is sampled from the following mixture:

$$z_i \sim \sum_{k=0}^1 p(s_i = k) p(z_i | s_i = k) = c_i f_1(z_i) + (1 - c_i) f_0(z_i), \quad (2.1)$$

where s_i is a latent variable indicating if the voxel i belongs to the group of null features ($s_i = 0$) or the group of non-null ones ($s_i = 1$), $c_i = p(s_i = 1) =$

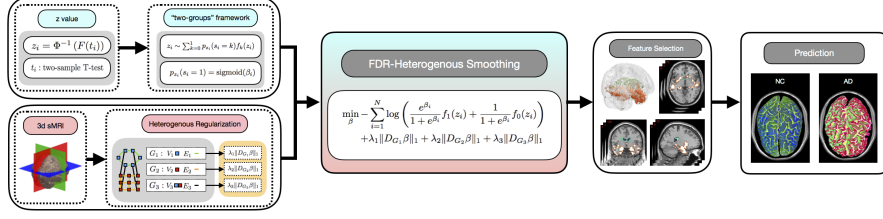


Fig. 2. Illustration of FDR-HS model.

$\text{sigmoid}(\beta_i) = e^{\beta_i} / (1 + e^{\beta_i})$ and $z_i = \Phi^{-1}(F_{N-2}(t_i))$ with t_i computed by two-sample t -test. Correspondingly, $f_0(\cdot)$ is density function of nulls, i.e. uncorrelated with AD and $f_1(\cdot)$ is that of non-nulls, i.e. procedural bias and lesions. The loss function can thus be defined as negative log-likelihood of z_i :

$$\ell(\beta) = - \sum_{i=1}^N \log \left(\frac{e^{\beta_i}}{1 + e^{\beta_i}} f_1(z_i) + \frac{1}{1 + e^{\beta_i}} f_0(z_i) \right) \quad (2.2)$$

which can be viewed as logistic regression (when f_0 and f_1 are replaced with binaries, as (2.6)) with identity design matrix since (2.1) proceeds voxel-by-voxel. Hence, it does not have the problem of multicollinearity.

Selecting Features. To select features, we compute the posterior distribution of s_i conditioned on z_i and $\hat{\beta}_i$ (estimated β_i) and features with

$$p(s_i = 0 | z_i, \hat{\beta}_i) = \frac{(1 - \hat{c}_i) f_0(z_i)}{\hat{c}_i f_1(z_i) + (1 - \hat{c}_i) f_0(z_i)} < \gamma \quad (\hat{c}_i = e^{\hat{\beta}_i} / (1 + e^{\hat{\beta}_i})) \quad (2.3)$$

are selected. The $\gamma \in (0, 1)$ is pre-setting threshold parameter.

Heterogenous Spatial Smoothing. However, (2.1) may lose spatial structure of non-nulls, especially lesion features. Besides, note that the procedural bias and lesion features are heterogenous in terms of volumetric change and level of spatial coherence. Hence, to capture the spatial structure of heterogenous features, we split the graph of voxels which denotes as \mathbf{G} ⁸ into three subgraphs, i.e. $\mathbf{G} = \mathbf{G}_1 \cup \mathbf{G}_2 \cup \mathbf{G}_3$ with:

$$\mathbf{G}_1 = (\mathbf{V}_1, \mathbf{E}_1), \quad \mathbf{V}_1 = \{i : z_i \leq 0\}, \quad \mathbf{E}_1 = \{(i, j) \in \mathbf{E} : z_i \leq 0, z_j \leq 0\} \quad (2.4a)$$

$$\mathbf{G}_2 = (\mathbf{V}_2, \mathbf{E}_2), \quad \mathbf{V}_2 = \{i : z_i > 0\}, \quad \mathbf{E}_2 = \{(i, j) \in \mathbf{E} : z_i > 0, z_j > 0\} \quad (2.4b)$$

$$\mathbf{G}_3 = (\mathbf{V}_3, \mathbf{E}_3), \quad \mathbf{V}_3 = \mathbf{V}_1 \cup \mathbf{V}_2, \quad \mathbf{E}_3 = \{(i, j) \in \mathbf{E} : z_i > 0, z_j \leq 0\} \quad (2.4c)$$

where \mathbf{G}_1 denotes the subgraph restricted on enlarged voxels (procedural bias since -1 denotes AD); \mathbf{G}_2 denotes the subgraph restricted on degenerate voxels (lesion features); \mathbf{G}_3 denotes the bipartite graph with the edges connecting enlarged and degenerate voxels. The optimization function can be redefined as:

$$g(\beta) = \ell(\beta) + \lambda_{pro} \|D_{\mathbf{G}_1} \beta\|_1 + \lambda_{les} \|D_{\mathbf{G}_2} \beta\|_1 + \lambda_{pro-les} \|D_{\mathbf{G}_3} \beta\|_1 \quad (2.5)$$

⁸ Here $\mathbf{G} = (\mathbf{V}, \mathbf{E})$, where \mathbf{V} is the node set of voxels, \mathbf{E} is the edge set of voxel pairs in neighbor (e.g. 3-by-3-by-3).

where $D_{\mathbf{G}_k}\beta = \sum_{(i,j) \in \mathbf{E}_k} \beta_i - \beta_j$ for $k \in \{1, 2, 3\}$ denote graph difference operator on $\mathbf{G}_{k=1,2,3}$. By setting the group of regularization hyper-parameters $\{\lambda_{pro}, \lambda_{les}, \lambda_{pro-les}\}$ with different values, we can enforce spatial smoothness on three subgraphs at different level in a contrast to the traditional homogeneous regularization in [13]. The choice of each hyper-parameter, similar to [13], it is a trade-off between over-fitting and over-smoothing. Too small value tends to select features more than needed, while too large value will oversmooth hence the features are less clustered. Note that lesion features are more spatially coherent than procedural bias and they are located in different regions, the reasonable choice of regularization hyper-parameters tend to have $\lambda_{les} \leq \lambda_{pro} \leq \lambda_{pro-les}$.

Optimization. Note that the function (2.5) is not convex. Hence we adopted the same idea in [13] that introduced the latent variables s_i and $= 1$ if $z_i \sim f_1(z)$ and 0 if $z_i \sim f_0(z)$. The $\ell(\beta)$ and $g(\beta)$ are modified as:

$$\ell(\beta, s) = \sum_{i=1}^N \{\log(1 + e^{\beta_i}) - s_i \beta_i\} \quad (2.6)$$

$$g(\beta, s) = \ell(\beta, s) + \lambda_{pro} \|D_{\mathbf{G}_1}\beta\|_1 + \lambda_{les} \|D_{\mathbf{G}_2}\beta\|_1 + \lambda_{pro-les} \|D_{\mathbf{G}_3}\beta\|_1 \quad (2.7)$$

To solve (2.7), we can implement Expectation-Maximization (EM) algorithm to alternatively solve β and s . Suppose currently we are in the $(k+1)^{th}$ iteration.

In the E-step, we can estimate s_i by expectation value conditional on (β^k, z_i) : $\tilde{s}_i = E(s_i | \beta^k, z_i) = \frac{c_i^k f_1(z_i)}{c_i^k f_1(z_i) + (1 - c_i^k) f_0(z_i)}$.

In the M-step, we plug \tilde{s}_i into (2.7), denote $\tilde{D}_{\mathbf{G}} = \left[D_{\mathbf{G}_1}^T, \frac{\lambda_{les}}{\lambda_{pro}} D_{\mathbf{G}_2}^T, \frac{\lambda_{pro-les}}{\lambda_{pro}} D_{\mathbf{G}_3}^T \right]^T$ and expand $\ell(\beta | \tilde{s}^k)$ using a second-order Taylor approximation at the β^k . Then the M-step turns into a generalized lasso problem with square loss:

$$\min_{\beta} \frac{1}{2} \|\tilde{y} - \tilde{X}\beta\|_2^2 + \lambda_{pro} \|\tilde{D}_{\mathbf{G}}\beta\|_1 \quad (2.8)$$

where $\tilde{X} = \text{diag}\{\sqrt{w_1}, \dots, \sqrt{w_p}\}$ and $\tilde{y}_i = \sqrt{w_i} (\beta_i^k - \nabla_{\beta} \ell(\beta | \tilde{s}_i^k)|_{\beta^k} / w_i)$ with $w_i = \nabla_{\beta}^2 \ell(\beta | \tilde{s}_i)|_{\beta^k}$. Note that X and $\tilde{D}_{\mathbf{G}}$ are sparse matrices, hence (2.8) can be efficiently solved by Alternating Direction Method of Multipliers (ADMM) [6] which has a complexity of $O(p \log p)$.

Estimation of f_0 and f_1 . Before the iteration, we need to estimate $f_0(z)$ and $f_1(z)$. The marginal distribution of z can be regarded as mixture models with p components: $z \sim \frac{1}{p} \sum_{i=1}^p g_i(z)$, $g_i(z) = p(s_i) p(z | s_i) = c_i f_1(z) + (1 - c_i) f_0(z)$. Hence, the marginal distribution of z is $f(z) = \bar{c} f_1(z) + (1 - \bar{c}) f_0(z)$, which is equivalent to LocalFDR [7]. We can therefore implement the CM (Central Matching) [7] method to estimate $\{f_0(z), \bar{c}\}$ and kernel density to estimate $f(z)$. The $f_1(z)$ can thus be given as $(f(z) - f_0(z)\bar{c}) / (1 - \bar{c})$.

3 Experimental Results

In this section, we evaluate the proposed method by applying it on the ADNI database <http://adni.loni.ucla.edu>. The database is split into 1.5T and 3.0T

(namely 15 and 30) MRI scanner magnetic field strength datasets. The 15 dataset contains 64 AD, 110 MCI (Mild Cognitive Impairment) and 90 NC, while the 30 dataset contains 66 AD and 110 NC. After applying DARTEL VBM [2] preprocessing pipeline on the data with scale of $4 \times 4 \times 4$ mm³ voxel size, there are in total 20,091 voxels with average values in GM population on template greater than 0.1 and they are served as input features. We designed experiments on 1.5T AD/NC, 1.5T MCI/NC and 3.0T AD/NC tasks, namely 15ADNC, 15MCINC and 30ADNC, respectively.

3.1 Prediction Results

To test the efficacy of selected features by FDR-HS and compare it with other univariate models (as listed in Table 1), we feed them into elastic net classifier, which has been one of the state-of-the-arts in the prediction of neuroimage data [11]. The hyper-parameters are determined by grid-search. In details, the threshold hyper-parameter of p-value in T-test and q-value in BH_q are optimized through $\{0.001, 0.01, 0.02, 0.05, 0.1\}$; the threshold hyper-parameter for choosing non-nulls, i.e. γ for FDR-HS (2.3) and the counterpart of LocalFDR [7], are chosen from $\{0.1, 0.2, \dots, 0.5\}$. Besides, the regularization parameters λ_{pro} , λ_{les} and $\lambda_{pro-les}$ of FDR-HS are ranged in $\{0.1, 0.2, \dots, 2\}$. For elastic net, the regularization parameter is chosen from $\{0.1, 0.2, \dots, 2, 5, 10\}$; the mixture parameter α is from $\{0, 0.01, \dots, 1\}$. Moreover, we compare our model to GSplit LBI and elastic net, adopting the same optimized strategy for hyper-parameters in [12] (the top 300 negative voxels are identified as procedural bias [12]) and those of elastic net following after the univariate models, as mentioned above.

A 10-fold cross-validation strategy is applied and the classification results for all tasks are summarized in Table 1. As shown, our method yields better results than others in all cases, that includes: (1) FDR-HS can select features with more prediction power than other univariate models due to the ability to capture heterogeneous spatial patterns; (2) FDR-HS can achieve better classification results than multivariate methods in high dimensional settings, in which the non-nulls may be represented by other nulls that are highly correlated with them.

Table 1. Comparison between FDR-HS and others on 10-fold classification result

	Univariate + ElasticNet				Multivariate	
	T-test	BH_q [4]	LocalFDR [7]	FDR-HS	GSplit LBI [12]	Elastic Net [17]
15ADNC	89.61%	89.61%	87.01%	90.26%	85.06%	87.01%
15MCINC	70.50%	71.00%	73.50%	75.00%	72.50%	72.00%
30ADNC	88.64%	89.77%	89.77%	91.48%	89.77%	88.07%

3.2 Feature Selection Analysis

We used 2-d images of 30ADNC to visualize the features of all methods under the hyper-parameters that give the best accuracy. As shown in Fig. 3,

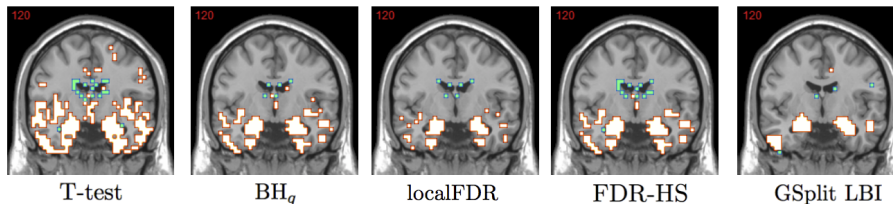


Fig. 3. The comparison of FDR-HS between others in terms of feature selection (30ADNC). Red denotes lesions; blue denotes procedural bias.

the lesion features selected by FDR-HS are located clustered in early damaged regions; while procedural bias are surrounding around lateral ventricle. Besides, such a result is given by $\lambda_{les} < \lambda_{pro} < \lambda_{pro-les}$, which agrees with that the larger value results in features with lower level of spatial coherence. In contrast, the lesions selected by T-test and BH_q are scattered and redundant; some procedural bias around lateral ventricle are missed by BH_q and LocalFDR. Moreover, GSplit LBI selected procedural bias on regions with CSF space less enlarged than lateral ventricle; besides, it ignored lesions located in medial temporal lobe, Thalamus and Fusiform etc., which are believed to be the early damaged regions [1,8].

Besides, we also evaluated the stability of selected features using multi-set Dice Coefficient (mDC) measurement defined in [16]. Larger mDC implies more stable feature selection. As shown in Table 2, our model can obtain more stable results than GSplit LBI which suffer the “collinearity” problem.

Table 2. Comparison between FDR-HS and others on stability (measured by mDC)

	T-test	BH_q	LocalFDR	FDR-HS	GSplit LBI
mDC ⁽⁺⁾ (Lesion features)	0.6705	0.6248	0.6698	0.6842	0.4598
mDC ⁽⁻⁾ (Procedural Bias)	0.6267	0.5541	0.5127	0.6540	0.3033

4 Conclusions

In this paper, a “two-groups” Empirical-Bayes model is proposed to stably and efficiently select interpretable heterogenous features in voxel-based neuroimage analysis. By modeling prior probability voxel-by-voxel and using a heterogeneous regularization, the model can avoid multicollinearity and exploit spatial patterns of features. With experiments on ADNI database, the features selected by our models have better interpretability and prediction power than others.

Acknowledgements. This work was supported in part by 973-2015CB351800, NSFC-61625201, 61527804, National Basic Research Program of China (Nos.

2015CB85600, 2012CB825501), NNSF of China (Nos. 61370004, 11421110001), HKRGC grant 16303817, Scientific Research Common Program of Beijing Municipal Commission of Education (No. KM201610025013) and grants from Tencent AI Lab, Si Family Foundation, Baidu BDI and Microsoft Research-Asia.

References

1. Aggleton, J.P., Pralus, A., Nelson, A.J., Hornberger, M.: Thalamic pathology and memory loss in early alzheimers disease: moving the focus from the medial temporal lobe to papez circuit. *Brain* 139(7), 1877–1890 (2016)
2. Ashburner, J.: A fast diffeomorphic image registration algorithm. *Neuroimage* 38(1), 95–113 (2007)
3. Ashburner, J., Friston, K.J.: Why voxel-based morphometry should be used. *Neuroimage* 14(6), 1238–1243 (2001)
4. Benjamini, Y., Hochberg, Y.: Controlling the false discovery rate: a practical and powerful approach to multiple testing. *Journal of the royal statistical society. Series B (Methodological)* pp. 289–300 (1995)
5. Bießmann, F., Dähne, S., Meinecke, F.C., Blankertz, B., Görden, K., Müller, K.R., Haufe, S.: On the interpretability of linear multivariate neuroimaging analyses: filters, patterns and their relationship. *Citeseer*
6. Boyd, S., Parikh, N., Chu, E., Peleato, B., Eckstein, J., et al.: Distributed optimization and statistical learning via the alternating direction method of multipliers. *Foundations and Trends® in Machine Learning* 3(1), 1–122 (2011)
7. Efron, B., Hastie, T.: *Computer age statistical inference: Algorithms. Evidence and Data Science*, Institute of Mathematical Statistics Monographs (2016)
8. Galton, C.J., Patterson, K., Graham, K., Lambon-Ralph, M., Williams, G., Antoun, N., Sahakian, B., Hodges, J.: Differing patterns of temporal atrophy in alzheimers disease and semantic dementia. *Neurology* 57(2), 216–225 (2001)
9. Haufe, S., Meinecke, F., Görden, K., Dähne, S., Haynes, J.D., Blankertz, B., Bießmann, F.: On the interpretation of weight vectors of linear models in multivariate neuroimaging. *Neuroimage* 87, 96–110 (2014)
10. Rudin, L.I., Osher, S., Fatemi, E.: Nonlinear total variation based noise removal algorithms. *Physica D: Nonlinear Phenomena* 60(1-4), 259–268 (1992)
11. Shen, L., Kim, S., Qi, Y., Inlow, M., Swaminathan, S., Nho, K., Wan, J., Risacher, S.L., Shaw, L.M., Trojanowski, J.Q., et al.: Identifying neuroimaging and proteomic biomarkers for mci and ad via the elastic net. In: *International Workshop on Multimodal Brain Image Analysis*. pp. 27–34. Springer (2011)
12. Sun, X., Hu, L., Yao, Y., Wang, Y.: Gsplit lbi: Taming the procedural bias in neuroimaging for disease prediction. In: *International Conference on Medical Image Computing and Computer-Assisted Intervention*. pp. 107–115. Springer (2017)
13. Tansey, W., Koyejo, O., Poldrack, R.A., Scott, J.G.: False discovery rate smoothing. *Journal of the American Statistical Association* (just-accepted) (2017)
14. Tu, Y.K., Kellett, M., Clerehugh, V., Gilthorpe, M.S.: Problems of correlations between explanatory variables in multiple regression analyses in the dental literature. *British dental journal* 199(7), 457 (2005)
15. Vaïter, S., Peyré, G., Dossal, C., Fadili, J.: Robust sparse analysis regularization. *IEEE Transactions on Information Theory* 59(4), 2001–2016 (2013)
16. Xin, B., Hu, L., Wang, Y., Gao, W.: Stable feature selection from brain smri. *AAAI* pp. 1910–1916 (2014)

17. Zou, H., Hastie, T.: Regularization and variable selection via the elastic net. *Journal of the Royal Statistical Society: Series B (Statistical Methodology)* 67(2), 301–320 (2005)

Supplementary Information

A Multicollinearity problem

One can implement sparse multivariate models for feature selection and classification by minimizing the penalized optimization function. Particularly, n^2 GFL [16] was proposed to stably capture the degenerate voxels by harnessing the sparsity and geometrically clustering properties under the $\beta \geq 0$ constraint and regularization function $\Omega(\beta) = \|D\beta\|_1$ with $D = [I; \rho D_G]$.⁹ On the basis of this, GSplit LBI was proposed to capture additional procedural bias via a variable splitting scheme.

However, such multivariate models suffer from the multicollinearity problem, i.e. high correlation among features, including the following aspects in details: (1) the collinearity between non-nulls and nulls can make the irrepresentable condition of genlasso which ensures the successfully recovery of the true support set [15] hard to satisfy. Such problem can violate the non-nulls to be selected; (2) the collinearity among non-nulls of sparsity model such as lasso/genlasso tends to only select one feature/region among correlated ones. (3) the procedural bias may be represented by other variables which are highly correlated with them due to the ‘‘collinearity’’ between non-nulls and nulls during minimization of General Linear Model (GLM). Specifically, the general penalized optimization function of the multivariate model is:

$$(\beta, \beta_0) = \arg_{(\beta, \beta_0)} \min \ell(\beta, \beta_0) + \lambda \Omega(\beta) \quad (\text{A.1})$$

where $\ell(\beta, \beta_0) = \frac{1}{N} \sum_{i=1}^N \log(1 + e^{y_i \cdot (\beta_0 + x_i^T \beta)}) - y_i \cdot (\beta_0 + x_i^T \beta)$ with β_0 denoting the bias parameter and $\Omega(\beta)$ is the regularization function. Different choice of $\Omega(\beta)$ leads to different model.

Since GSplit LBI and genlasso enforce same sparsity regularizations on lesion features, we firstly discuss the problem of genlasso under high dimensional space: (1) the irrepresentable condition which ensures the model selection consistency (i.e. successfully recover the true support set) is not easy to satisfy (2) only select one feature/cluster among correlated ones.

To understand (1), note in [15] that under linear model the necessary condition for genlasso to satisfy model selection consistency is that $IC_1 < 1$. When $D = I$, the slightly stronger version of this condition is $\|X_{S^c}^T X_S (X_S^T X_S)^{-1}\|_1 < 1$ where S denotes the true support set (lesion voxels). Such irrepresentable condition implies the ‘‘decorrelated’’ property of S and S^c . However, such condition is hard to satisfy under high dimensional space since covariates are more easier to be correlated.

⁹ Here $D_G \beta = \sum_{(i,j) \in E} \beta_i - \beta_j$ denotes a graph difference operator on $\mathbf{G} = (\mathbf{V}, \mathbf{E})$, where \mathbf{V} is the node set of voxels, \mathbf{E} is the edge set of voxel pairs in neighbour (e.g. 3-by-3-by-3).

To see (2), note in [17] that the lasso only selects one feature among a group of correlated ones. We claim that genlasso also suffers from this limitation. Specifically, it can be shown in Lemma 1 that the Total Variation regularization of genlasso tends to select only single region among a group of correlated ones.

Lemma 1. *Let $\mathbf{G}_{S_1} = (\mathbf{V}_{S_1}, \mathbf{E}_{S_2})$ and $\mathbf{G}_{S_2} = (\mathbf{V}_{S_2}, \mathbf{E}_{S_1})$ denotes two subgraphs (regions) that are not connected with other nodes in \mathbf{V} , i.e.*

$$D_G = \begin{bmatrix} D_{S_1} & & \\ & D_{S_2} & \\ & & D_{S_1^c \cap S_2^c} \end{bmatrix}$$

where $S_1 \subset \{1, \dots, p\}$, $S_2 \subset \{1, \dots, p\}$, $|S_1| = |S_2|$ and $S_1 \cap S_2 = \emptyset$. If $D_{S_1} = D_{S_2}$, $X_{S_1} = X_{S_2}$ and $\hat{\beta}$ is the solution of A.1 with $\Omega\beta = \|D_G\beta\|_1$, then $\hat{\beta}^*$ is the other solution where

$$\hat{\beta}_k^* = \begin{cases} \hat{\beta}_k & k \in S_1^c \cap S_2^c \\ \left(\hat{\beta}_k + \hat{\beta}_{k(S_2)} \right) \cdot s & k \in S_1 \\ \left(\hat{\beta}_{k(S_1)} + \hat{\beta}_k \right) \cdot (1 - s) & k \in S_2 \end{cases}$$

for any $s \in [0, 1]$, where $k(S_{t=1,2})$ are indexes such that $X_k = X_{k(S_{t=1,2})}$ for $k \in S_{t=2,1}$.

Proof. It can be easily verified from the definition of A.1.

Now we discuss the problem of the procedural bias in GSplit LBI, i.e. the procedural bias may be represented by other variables which are highly correlated with them due to the ‘‘collinearity’’. Note that to select procedural bias, GSplit LBI adopts an variable splitting scheme $\|D\beta - \gamma\|_2^2$ by introducing an augmented variable γ , the loss function is redefined as:

$$\ell(\beta_0, \beta, \gamma) = \ell(\beta_0, \beta) + \frac{1}{2\nu} \|D\beta - \gamma\|_2^2 \quad (\text{A.2})$$

and implement it by the following iterative algorithm:

$$\beta_0^{k+1} = \beta_0^k - \kappa\alpha \nabla_{\beta_0} \ell(\beta_0^k, \beta^k, \gamma^k), \quad (\text{A.3a})$$

$$\beta^{k+1} = \beta^k - \kappa\alpha \nabla_{\beta} \ell(\beta_0^k, \beta^k, \gamma^k), \quad (\text{A.3b})$$

$$z^{k+1} = z^k - \alpha \nabla_{\gamma} \ell(\beta_0^k, \beta^k, \gamma^k), \quad (\text{A.3c})$$

$$\gamma_{\mathbf{V}}^{k+1} = \kappa \cdot \max(z_{\mathbf{V}}^{k+1} - 1, 0), \quad (\text{A.3d})$$

$$\gamma_{\mathbf{G}}^{k+1} = \kappa \cdot \text{sign} \max(|z_{\mathbf{G}}^{k+1}| - 1, 0), \quad (\text{A.3e})$$

$$\beta_{les}^{k+1} = (I - D_{S_{k+1}^c}^\dagger D_{S_{k+1}^c}) \beta^{k+1}, \quad (\text{A.3f})$$

where $S_k := \text{supp}(\gamma^k)$. Note that in A.3f, the β_{les} , which is the projection of β onto the support set of γ , is the estimator to capture lesion features. The elements

with comparably large magnitude among the remainder of such projection are regarded as procedural bias. However, under high dimensional data, such definition may suffer multicollinearity problem that the procedural bias are “submerged” or represented by other null variables that have high correlation with them. In detail, note that the procedural bias are less clustered than lesion features and also that in A.3b, when $\kappa \rightarrow \infty$, $\alpha \rightarrow 0$, we have $\beta^{k+1} \rightarrow \arg \min_{\beta} \ell(\beta_0^k, \beta, \gamma^k)$, i.e. minimizing GLM model, it can then be shown in the following lemma that the algorithm may choose null variables while the procedural bias may not be successfully recovered.

Lemma 2. Denotes the set of index of procedural bias as S_{pro} . Assume $i \in S_{pro}$ and $\{j_1, \dots, j_m\} \subset S_{pro}^c$ are isolated points satisfying (1) $\gamma_{\{i, j_1, \dots, j_m\}}^k = 0$ and (2) $X_i = \sum_{k=1}^m X_{j_k} s_k$ for some $\{s_1, \dots, s_m\}$ such that $\sum_{k=1}^m s_k = 1$ and $s_k > 0$ for $k \in \{1, \dots, m\}$. If $\hat{\beta}^*$ minimizes $\ell(\beta_0^k, \beta, \gamma^k)$, then $\hat{\beta}_i^* = \sum_{k=1}^m \hat{\beta}_{j_k}^* s_{j_k}$, which means $|\hat{\beta}_i^*| \leq \max\{|\hat{\beta}_{j_k}^*|\}_{k=1, \dots, m}$. Furthermore, if $|\hat{\beta}_{j_1}^*| = |\hat{\beta}_{j_2}^*| = \dots = |\hat{\beta}_{j_m}^*|$ does not hold, then $|\hat{\beta}_i^*| < \max\{|\hat{\beta}_{j_k}^*|\}_{k=1, \dots, m}$.

Proof. Since $\hat{\beta}^*$ minimizes $\ell(\beta_0^k, \beta, \gamma^k)$, then it’s easy to see that

$$\hat{\beta}_t^\alpha = \begin{cases} \alpha \hat{\beta}_i^* & t = i \\ (1 - \alpha) s_{j_k} \hat{\beta}_i^* + \hat{\beta}_{s_{j_k}}^* & t = s_{j_k} (k = 1, \dots, m) \\ \hat{\beta}_t^* & t \notin \{i, j_1, \dots, j_m\} \end{cases}$$

satisfies that $\ell(\beta_0^k, \hat{\beta}^\alpha) = \ell(\beta_0^k, \hat{\beta}^*)$ for any $\alpha \in [0, 1]$. Denote $\mathcal{I} = \{i, j_1, \dots, j_m\}$. Since \mathcal{I} corresponds to isolate points and $\gamma_{\mathcal{I}}^k = 0$, then

$$\arg \min_{\beta_{\mathcal{I}}} \ell(\beta_0^k, \beta_{\mathcal{I}}, \hat{\beta}_{\mathcal{I}^c}^*, \gamma^k) \iff \arg \min_{\beta_{\mathcal{I}}} \ell(\beta_0^k, \beta_{\mathcal{I}}, \hat{\beta}_{\mathcal{I}^c}^*) + \frac{1}{2\nu} \|\beta_{\mathcal{I}}\|_2^2$$

By computing the gradient of $\|\hat{\beta}^\alpha\|_2^2$ over α , it’s easy to see that $\hat{\beta}_{\mathcal{I}}^* = \hat{\beta}_{\mathcal{I}}^1 = \arg \min_{\beta_{\mathcal{I}}} \ell(\beta_0^k, \beta_{\mathcal{I}}, \hat{\beta}_{\mathcal{I}^c}^*) + \frac{1}{2\nu} \|\beta_{\mathcal{I}}\|_2^2$ only if $\hat{\beta}_i^* = \sum_{k=1}^m \hat{\beta}_{j_k}^* s_{j_k}$. Since $|\cdot|$ is an convex function and $\hat{\beta}_i^*$ is a convex combination of $\{\hat{\beta}_{j_k}^*\}_{k=1, \dots, m}$, we then have

$$|\hat{\beta}_i^*| \leq \sum_{k=1}^m s_k |\hat{\beta}_{j_k}^*| \leq \max\{|\hat{\beta}_{j_k}^*|\}_{k=1, \dots, m}$$

The last inequality can be dropped if $|\hat{\beta}_{j_1}^*| = |\hat{\beta}_{j_2}^*| = \dots = |\hat{\beta}_{j_m}^*|$ does not hold.

B Heterogenous Features

We mentioned that the procedural bias and lesion features are heterogenous in terms of volumetric change (enlarged v.s. atrophied) and spatial patterns (surroundingly distributed v.s. spatially cohesive). The heterogeneity in terms of

volumetric change is easy to understand, since the procedural bias commonly refer to enlarged GM voxels in voxel-based dementia analysis and lesion features refer to atrophied ones. To illustrate the heterogeneous levels of spatial coherence, we evaluate the edge density in 3D coordinate system by introducing 3D edge density (3dED) measurement for both selected lesions and procedural bias. In detail, $3dED$ is defined as:

$$3dED^\pm = \frac{1}{K} \sum_{k=1}^K \frac{|\{(i, j) \in E : i \in S_k^\pm, j \in S_k^\pm\}|}{\max_{\widehat{\mathbf{G}}_{3d}} \left\{ \left| \widehat{\mathbf{E}} \right| : \widehat{\mathbf{G}}_{3d} = (\widehat{\mathbf{V}}, \widehat{\mathbf{E}}), \left| \widehat{\mathbf{V}} \right| = |\{i : i \in S_k^\pm\}| \right\}} \quad (\text{B.1})$$

where S_k^\pm denote the support set of lesion features and procedural bias in the k -th fold, respectively. For each fold k , we need to compute:

$$\max_{\widehat{\mathbf{G}}_{3d}} \left\{ \left| \widehat{\mathbf{E}} \right| : \widehat{\mathbf{G}}_{3d} = (\widehat{\mathbf{V}}, \widehat{\mathbf{E}}), \left| \widehat{\mathbf{V}} \right| = |\{i : i \in S_k^\pm\}| \right\}$$

For the graphs with p voxels which are embedded in 3-d coordinate space, the maximum number of edges is equal to:

$$\max_{(c_1, c_2, c_3, s_1, s_2, r) \in \mathcal{S}_p^{3d}} \{3c_1c_2c_3 - c_1c_2 - c_1c_3 - c_2c_3 + 2r_1r_2 - r_1 - r_2 + l\}$$

where

$$\begin{aligned} \mathcal{S}_p^{3d} = \{ & [c_1, c_2, c_3, r_1, r_2, l] \in \mathbb{R}_{1 \times 6} : c_1c_2c_3 + r_1r_2 + l = p, r \leq \max\{r_1, r_2\}, \\ & \{r_1r_2 + r \leq c_1c_2, r_1 \leq c_1, r_2 \leq c_2\} \text{ or } \{r_1r_2 + l \leq c_1c_3, r_1 \leq c_1, r_2 \leq c_3\} \\ & \text{ or } \{r_1r_2 + l \leq c_2c_3, r_1 \leq c_2, r_2 \leq c_3\} \} \end{aligned}$$

where $\mathbb{R}^+ = \{x \in \mathbb{R}, x \geq 0\}$. Besides, the c_1, c_2, c_3 can be taken as length, width and height of a cube, $r_1r_2 + l$ are the remainder of p for a cube (c_1, c_2, c_3). The r_1, r_2 can be taken as the length and width of the rectangle which is located on one of the surfaces of (c_1, c_2, c_3). The l is the residual of $p - c_1c_2c_3$ for rectangle (r_1, r_2).

According to B.1, the procedural bias are turned to be selected much less clustered than lesion features by all univariate models, e.g. the BH_q yields 0.4677 for lesion features and 0.1621 for procedural bias; while localFDR has 0.4662 and 0.1699; FDR-HS has 0.5365 and 0.2535, which validates the heterogenous assumption in terms of the level of spatial coherence.

C IDS of ADNI subject used in our experiments

Subject	ID	Class	Subject	ID	Class	Subject	ID	Class
123_S_0094	9655	15AD	137_S_0158	11127	15MCI	014_S_0558	17400	15NC
123_S_0088	9788	15AD	128_S_0225	11179	15MCI	021_S_0647	17668	15NC
098_S_0149	10146	15AD	136_S_0107	11227	15MCI	137_S_0686	17813	15NC

032_S.0147	10404	15AD	032_S.0214	11280	15MCI	032_S.0677	17820	15NC
123_S.0162	10962	15AD	005_S.0222	11299	15MCI	002_S.0685	18211	15NC
128_S.0216	11101	15AD	027_S.0179	11348	15MCI	094_S.0711	18589	15NC
128_S.0167	11203	15AD	021_S.0231	11430	15MCI	127_S.0684	18896	15NC
005_S.0221	11604	15AD	007_S.0249	11544	15MCI	033_S.0734	19155	15NC
014_S.0328	12327	15AD	098_S.0269	11615	15MCI	033_S.0741	19258	15NC
007_S.0316	12616	15AD	130_S.0289	11850	15MCI	094_S.0692	19567	15NC
021_S.0343	12979	15AD	021_S.0273	11942	15MCI	009_S.0751	20013	15NC
014_S.0356	13004	15AD	007_S.0293	11982	15MCI	116_S.0648	20370	15NC
032_S.0400	13525	15AD	031_S.0294	12065	15MCI	129_S.0778	20543	15NC
116_S.0370	14122	15AD	021_S.0276	12092	15MCI	029_S.0824	23213	15NC
127_S.0431	15497	15AD	128_S.0227	12119	15MCI	116_S.0657	23350	15NC
031_S.0554	15994	15AD	027_S.0256	12250	15MCI	006_S.0731	23468	15NC
128_S.0517	16150	15AD	130_S.0285	12424	15MCI	029_S.0845	24249	15NC
116_S.0487	16377	15AD	098_S.0288	12654	15MCI	009_S.0862	25128	15NC
002_S.0619	16392	15AD	007_S.0344	12697	15MCI	098_S.0896	25255	15NC
131_S.0497	16666	15AD	021_S.0332	12862	15MCI	033_S.0923	25427	15NC
021_S.0642	17632	15AD	128_S.0258	13085	15MCI	130_S.0886	25455	15NC
033_S.0739	19175	15AD	027_S.0307	13281	15MCI	006_S.0498	25790	15NC
100_S.0743	19585	15AD	123_S.0390	13315	15MCI	052_S.0951	26642	15NC
033_S.0724	19772	15AD	031_S.0351	13783	15MCI	130_S.0969	26688	15NC
128_S.0740	19990	15AD	021_S.0424	13909	15MCI	021_S.0984	27056	15NC
021_S.0753	20169	15AD	053_S.0389	13938	15MCI	024_S.0985	27607	15NC
137_S.0796	23112	15AD	094_S.0434	13964	15MCI	024_S.1063	28111	15NC
029_S.0836	23231	15AD	068_S.0401	14161	15MCI	033_S.1098	30304	15NC
100_S.0747	23581	15AD	131_S.0409	14240	15MCI	010_S.0472	30481	15NC
127_S.0754	23787	15AD	116_S.0361	14296	15MCI	137_S.0972	31702	15NC
012_S.0803	24863	15AD	132_S.0339	14367	15MCI	033_S.1086	32054	15NC
033_S.0889	25026	15AD	037_S.0377	14405	15MCI	130_S.1200	36281	15NC
126_S.0891	25172	15AD	027_S.0485	14928	15MCI	116_S.1232	37848	15NC
005_S.0929	25645	15AD	027_S.0408	14964	15MCI	027_S.0120	10933	15NC
006_S.0547	25816	15AD	137_S.0481	15044	15MCI	068_S.0127	11133	15NC
002_S.0955	26170	15AD	027_S.0417	15148	15MCI	068_S.0210	11235	15NC
130_S.0956	27032	15AD	053_S.0507	15315	15MCI	136_S.0186	11335	15NC
053_S.1044	27782	15AD	094_S.0531	15431	15MCI	009_S.0842	24339	15NC
133_S.1055	29381	15AD	033_S.0567	15459	15MCI	029_S.0843	24406	15NC
100_S.1062	29579	15AD	127_S.0394	15510	15MCI	032_S.1169	34067	15NC
029_S.1056	30618	15AD	033_S.0514	15605	15MCI	018_S.0055	9136	15NC
029_S.0999	31239	15AD	033_S.0513	15622	15MCI	100_S.0015	8390	30NC
006_S.0653	31252	15AD	130_S.0460	15711	15MCI	136_S.0196	14236	30NC
014_S.1095	31576	15AD	098_S.0542	15848	15MCI	136_S.0086	14712	30NC
094_S.1090	31678	15AD	007_S.0414	15875	15MCI	018_S.0369	15110	30NC
021_S.1109	31784	15AD	031_S.0568	15885	15MCI	131_S.0441	15959	30NC
024_S.1171	35190	15AD	037_S.0501	15916	15MCI	032_S.0479	16652	30NC
133_S.1170	35211	15AD	037_S.0552	15970	15MCI	018_S.0425	17168	30NC
031_S.1209	36178	15AD	130_S.0423	16196	15MCI	126_S.0405	17177	30NC
130_S.1201	36269	15AD	014_S.0557	16304	15MCI	005_S.0553	17619	30NC
027_S.1081	37145	15AD	033_S.0511	16314	15MCI	126_S.0605	17639	30NC
126_S.1221	37339	15AD	130_S.0449	16351	15MCI	005_S.0602	19615	30NC
029_S.1184	37350	15AD	027_S.0461	16467	15MCI	012_S.1009	28962	30NC

027_S.1254	37859	15AD	128_S.0608	16503	15MCI	012_S.1212	37403	30NC
130_S.1290	38395	15AD	128_S.0611	16766	15MCI	007_S.1206	37761	30NC
033_S.1285	38593	15AD	053_S.0621	16864	15MCI	068_S.1191	38370	30NC
033_S.1283	38617	15AD	037_S.0566	16886	15MCI	007_S.1222	38482	30NC
033_S.1308	40114	15AD	037_S.0539	17018	15MCI	094_S.1241	41449	30NC
024_S.1307	41527	15AD	137_S.0443	17030	15MCI	002_S.1261	41799	30NC
007_S.1339	42344	15AD	005_S.0546	17056	15MCI	002_S.1280	41806	30NC
130_S.1337	42930	15AD	137_S.0631	17109	15MCI	052_S.1251	43812	30NC
127_S.1382	45060	15AD	027_S.0644	17157	15MCI	100_S.1286	45761	30NC
094_S.1397	51790	15AD	133_S.0629	17596	15MCI	094_S.1267	46457	30NC
094_S.1402	54220	15AD	021_S.0626	17687	15MCI	131_S.1301	49328	30NC
136_S.0299	15181	30AD	098_S.0667	17702	15MCI	098_S.4003	224603	30NC
136_S.0426	16172	30AD	052_S.0671	17849	15MCI	098_S.4018	228788	30NC
018_S.0335	16560	30AD	014_S.0563	17876	15MCI	031_S.4021	229148	30NC
136_S.0300	16719	30AD	007_S.0698	18363	15MCI	012_S.4026	238532	30NC
018_S.0633	19093	30AD	133_S.0638	18672	15MCI	098_S.4050	238615	30NC
012_S.0689	19210	30AD	033_S.0723	19014	15MCI	016_S.4097	243556	30NC
126_S.0606	20487	30AD	032_S.0718	19035	15MCI	016_S.4952	337793	30NC
131_S.0691	20681	30AD	126_S.0708	19089	15MCI	016_S.4121	246002	30NC
005_S.0814	24734	30AD	128_S.0715	19225	15MCI	006_S.4150	249403	30NC
002_S.0816	25405	30AD	033_S.0725	19404	15MCI	127_S.4148	250137	30NC
127_S.0844	29230	30AD	137_S.0669	19419	15MCI	003_S.4119	250894	30NC
002_S.1018	33832	30AD	116_S.0649	19516	15MCI	127_S.4198	254320	30NC
031_S.4024	228879	30AD	130_S.0505	19701	15MCI	002_S.4213	254582	30NC
016_S.4009	240946	30AD	137_S.0722	19707	15MCI	031_S.4218	255978	30NC
094_S.4089	242719	30AD	126_S.0709	19754	15MCI	002_S.4225	257270	30NC
006_S.4153	248517	30AD	128_S.0770	19907	15MCI	002_S.4262	259653	30NC
003_S.4136	250173	30AD	014_S.0658	20003	15MCI	941_S.4100	259781	30NC
003_S.4152	253760	30AD	137_S.0668	20202	15MCI	002_S.4264	259796	30NC
098_S.4215	255843	30AD	137_S.0800	20500	15MCI	021_S.4276	260047	30NC
098_S.4201	256178	30AD	002_S.0782	20519	15MCI	029_S.4290	260425	30NC
006_S.4192	258594	30AD	130_S.0783	20794	15MCI	098_S.4275	261459	30NC
019_S.4252	258947	30AD	116_S.0752	23097	15MCI	094_S.4234	261531	30NC
024_S.4280	261332	30AD	068_S.0802	23389	15MCI	018_S.4257	262076	30NC
094_S.4282	261855	30AD	133_S.0792	23444	15MCI	136_S.4269	264215	30NC
029_S.4307	267595	30AD	006_S.0675	23644	15MCI	029_S.4279	265980	30NC
016_S.4353	267937	30AD	031_S.0821	23658	15MCI	021_S.4335	266174	30NC
109_S.4378	270669	30AD	133_S.0771	23876	15MCI	130_S.4343	266217	30NC
126_S.4494	281605	30AD	133_S.0727	23939	15MCI	018_S.4349	266625	30NC
127_S.4500	283515	30AD	027_S.0835	24138	15MCI	129_S.4369	267405	30NC
007_S.4568	287472	30AD	031_S.0830	24281	15MCI	130_S.4352	267711	30NC
006_S.4546	287994	30AD	100_S.0035	8120	15NC	129_S.4371	268462	30NC
130_S.4589	291219	30AD	100_S.0047	8899	15NC	018_S.4313	268930	30NC
016_S.4591	292433	30AD	010_S.0067	9093	15NC	019_S.4367	269273	30NC
016_S.4583	294209	30AD	018_S.0043	9324	15NC	007_S.4387	269929	30NC
014_S.4615	294334	30AD	100_S.0069	9417	15NC	036_S.4389	270462	30NC
130_S.4641	295961	30AD	032_S.0095	9680	15NC	003_S.4350	270999	30NC
130_S.4660	300034	30AD	123_S.0072	9752	15NC	129_S.4422	272184	30NC
019_S.4549	300335	30AD	007_S.0070	10027	15NC	018_S.4399	272231	30NC
126_S.4686	300818	30AD	131_S.0123	10043	15NC	018_S.4399	272231	30NC

005_S.4707	304663	30AD	123_S.0106	10126	15NC	021_S.4421	273564	30NC
021_S.4718	304749	30AD	027_S.0118	11370	15NC	029_S.4383	273993	30NC
018_S.4733	306069	30AD	098_S.0172	11398	15NC	003_S.4441	277108	30NC
130_S.4730	306384	30AD	130_S.0232	11567	15NC	136_S.4433	278511	30NC
137_S.4756	307118	30AD	005_S.0223	11645	15NC	006_S.4449	279470	30NC
027_S.4801	314034	30AD	123_S.0113	11714	15NC	031_S.4474	280369	30NC
027_S.4802	317195	30AD	128_S.0230	11806	15NC	007_S.4488	281560	30NC
006_S.4867	322012	30AD	137_S.0283	12028	15NC	006_S.4485	281882	30NC
016_S.4887	325649	30AD	128_S.0245	12242	15NC	010_S.4345	282005	30NC
007_S.4911	328196	30AD	128_S.0272	12313	15NC	031_S.4496	282638	30NC
021_S.4924	331257	30AD	128_S.0229	12459	15NC	098_S.4506	282934	30NC
137_S.4756	332930	30AD	021_S.0337	12466	15NC	094_S.4459	283445	30NC
127_S.4940	335512	30AD	098_S.0171	10818	15NC	094_S.4460	283573	30NC
027_S.4938	336926	30AD	072_S.0315	12559	15NC	010_S.4442	283915	30NC
027_S.4962	338558	30AD	137_S.0301	12584	15NC	007_S.4516	284424	30NC
130_S.4982	341787	30AD	002_S.0295	13722	15NC	029_S.4385	285589	30NC
130_S.4984	342274	30AD	037_S.0327	13802	15NC	094_S.4503	286222	30NC
130_S.4971	342338	30AD	027_S.0403	14146	15NC	073_S.4559	286553	30NC
127_S.4992	342697	30AD	137_S.0459	14178	15NC	021_S.4558	287527	30NC
019_S.5012	343916	30AD	002_S.0413	14437	15NC	109_S.4499	288999	30NC
019_S.5019	345663	30AD	068_S.0473	14483	15NC	100_S.4469	289564	30NC
002_S.5018	346242	30AD	116_S.0360	14623	15NC	100_S.4511	289653	30NC
127_S.5028	346696	30AD	133_S.0488	14838	15NC	012_S.4545	290413	30NC
130_S.4997	347410	30AD	133_S.0493	14848	15NC	053_S.4578	290814	30NC
005_S.5038	351432	30AD	014_S.0520	15299	15NC	127_S.4604	291523	30NC
127_S.5056	353203	30AD	014_S.0519	15323	15NC	007_S.4620	293938	30NC
127_S.5058	354636	30AD	116_S.0382	15347	15NC	127_S.4645	295590	30NC
007_S.0128	10007	15MCI	128_S.0500	15366	15NC	002_S.4270	260581	30NC
010_S.0161	10077	15MCI	010_S.0419	15415	15NC	013_S.4579	296776	30NC
021_S.0141	10173	15MCI	131_S.0436	15674	15NC	013_S.4580	296859	30NC
127_S.0112	10419	15MCI	128_S.0522	15821	15NC	012_S.4642	296878	30NC
128_S.0135	10431	15MCI	033_S.0516	15860	15NC	012_S.4643	297693	30NC
128_S.0138	10438	15MCI	002_S.0559	15948	15NC	029_S.4585	298523	30NC
098_S.0160	10466	15MCI	014_S.0548	16024	15NC	013_S.4616	300089	30NC
123_S.0108	10738	15MCI	128_S.0545	16090	15NC	029_S.4652	300886	30NC
037_S.0150	10773	15MCI	010_S.0420	17078	15NC	137_S.4632	301677	30NC
027_S.0116	10783	15MCI	126_S.0506	17184	15NC	094_S.4649	302926	30NC
128_S.0188	10897	15MCI	005_S.0610	17303	15NC	016_S.4638	305882	30NC
014_S.0169	10987	15MCI	006_S.0484	17377	15NC	013_S.4731	308178	30NC
021_S.0178	10993	15MCI	031_S.0618	16598	15NC	136_S.4726	308396	30NC
128_S.0205	11011	15MCI	016_S.4951	337692	30NC	016_S.4688	310327	30NC
128_S.0200	11012	15MCI	003_S.4839	319414	30NC	019_S.4835	315857	30NC
037_S.0182	11121	15MCI	003_S.4900	325729	30NC	127_S.4843	316771	30NC
003_S.4840	319427	30NC	003_S.4872	321376	30NC			